Phase chaos generation and security enhancement by introducing fine-controllable dispersion

IOP Publishing Journal of Optics
J. Opt. **20** (2018) 024004 (5pp) https://doi.org/10.1088/2040-8986/aa9e1d

Phase chaos generation and security enhancement by introducing fine-controllable dispersion

Lilin Yi[1,3], Junxiang Ke[1], Guangqiong Xia[2] and Weisheng Hu[1]

[1] State Key Lab of Advanced Optical Communication Systems and Networks, Shanghai Institute for Advanced Communication and Data Science, Shanghai Jiao Tong University, Shanghai 200240, People's Republic of China
[2] School of Physics, Southwest University, Chongqing 400715, People's Republic of China

E-mail: lilinyi@sjtu.edu.cn

Received 30 August 2017, revised 14 November 2017
Accepted for publication 29 November 2017
Published 8 January 2018

Abstract

For the first time, we experimentally demonstrate phase chaos generation by introducing a fine-controllable dispersion module into the feedback-delayed loop. To study the effect of this specific nonlinearity, we demonstrate the nonlinear dynamics evolution route in terms of the dependence of dispersion and feedback gain parameters by both experiment and simulation, which show good agreement. We also investigate the synchronization error variation with the dispersion mismatch to evaluate the security level of the proposed phase chaos system. The results show that the proposed approach can simultaneously simplify the phase chaos synchronization and enhance the key space, which has potential to be used in high-speed chaotic optical communications.

Keywords: phase chaos, dispersion, optical security and encryption

(Some figures may appear in colour only in the online journal)

Chaos systems have become a promising hardware encryption method in optical communications since the first demonstration of chaos synchronization in 1990 [1]. The lasers and modulators are the two main components to generate chaos via delayed-feedback [2–8]. From the viewpoint of practical applications, a modulator-based chaotic system is more feasible since the chaos synchronization is simplified compared with the laser-based chaotic system, where the chaos dynamics are very sensitive to the laser physical parameters. Using a Mach–Zehnder modulator (MZM)-based scheme, the first field trial of chaotic optical communications in Athens' metro-network has been successfully demonstrated to support a 2.4 Gb s^{-1} bit rate and 120 km transmission distance [9]. However, the all-optical mixing process between the chaotic optical intensity carrier and the optical intensity binary data in the same wavelength will lead to undesired interference, therefore degrading the system performance [10]. Besides, the bias drift issue of the MZM will also complicate the chaos synchronization. So the scheme based on phase chaos has been proposed to overcome those drawbacks. In the first phase chaos configuration, a Mach–Zehnder interferometer (MZI) was used for the nonlinear transformation from phase to intensity inside the delayed-feedback loop [10], and the first 10 Gb s^{-1} field experiment of chaotic optical communications through phase chaos has been successfully demonstrated [11].

In this work, we propose a novel phase-chaos generator based on the nonlinear transformation from optical phase to intensity by using a fine-controllable tunable dispersion compensator (TDC). The evolution route to chaos has been clearly observed as the dispersion value is increased from 0 to 2100 ps nm^{-1}, which confirms the existence of deterministic phase chaos in this novel configuration. The simulation results match well with the experimental results, which also

[3] This article belongs to the special issue: Emerging Leaders, which features invited work from the best early-career researchers working within the scope of the *Journal of Optics*. Dr Lilin Yi was selected by the Editorial Board of the *Journal of Optics* as an Emerging Leader.

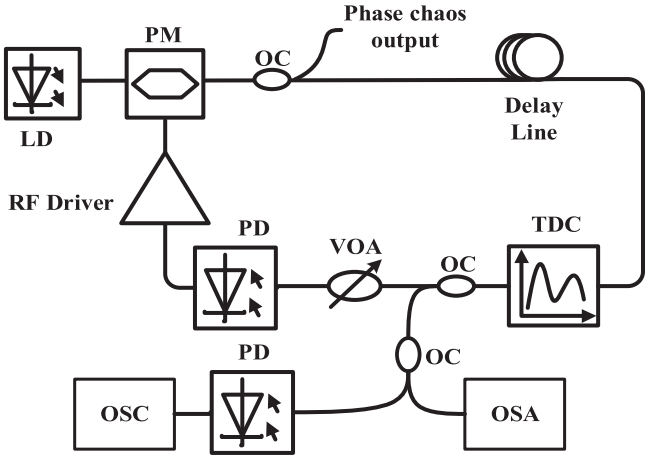

Figure 1. Experiment setup. LD is the laser diode, PM is the phase modulator, OC is the optical coupler, TDC is the tunable dispersion compensator, PD is the photodiode, VOA is the variable optical attenuator, OSC is the oscilloscope, and OSA is the optical spectrum analyzer.

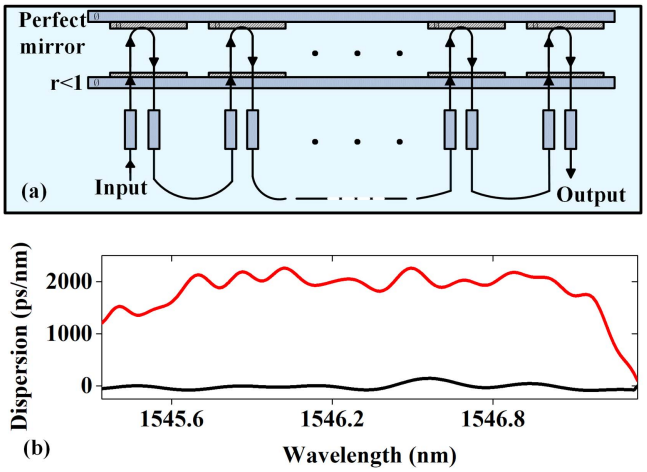

Figure 2. (a) Structure of the TDC module and (b) examples of the generated dispersion curve.

proves the validity of the phase chaos dynamics model. Thanks to the stable dispersion control of the TDC, phase chaos synchronization can be simplified. Furthermore, because the chaotic state can be sustained when the dispersion value is larger than 900 ps nm^{-1}, the dispersion curve precisely controlled by TDC can be used as an additional secure key, except for the cavity time delay, which greatly enhances the key space in chaotic optical communications. We hope the proposed phase chaos generation scheme opens a new window for high-speed and long-distance chaotic optical communications.

The experimental setup of the proposed scheme is illustrated in figure 1. A continuous-wave (CW) light with power of 10 dBm from a 1546.34 nm laser diode (LD) with a narrow linewidth of 100 KHz is launched into a broadband phase modulator (PM) with a bandwidth of 30 GHz and a half wave voltage of 3.9 V. The PM is used for the linear transformation between intensity and phase, and the optical phase of the injected light is modulated by the output of the radio-frequency (RF) driver with a 3 dB bandwidth of 30 KHz–10 GHz, a gain of 38 dB and maximum output peak to peak voltage of 20 V, while the intensity of the output light remains constant. Then, the output light propagates for a few meters of the optical fiber until it passes by the key component of the architecture, the TDC controlled by temperature, where the optical phase is nonlinearly converted into optical intensity by dispersion. Also, the optical output intensity signal of TDC is split into two beams, one beam is used for analysis, and the other beam is detected by a broadband amplified photodetector (PD) with a 3 dB bandwidth of 10 GHz and a responsivity of 400 mV mW^{-1}. Thus, the optical intensity signal is linearly converted into an electrical signal by PD when the injected optical power is less than 10 mW, and the feedback gain parameter can be controlled by tuning the injected optical power of PD through the variable optical attenuator (VOA). Then, the electrical output signal linearly amplified by the RF driver is fedback to the PM. The whole loop length is about 34.9 m, and the corresponding delay time is about 174.5 ns. By setting the dispersion value in a proper value through controlling the temperature of TDC, we can observe the abundant dynamics behavior of this feedback system. An optical spectrum analyzer (OSA) is utilized to observe the optical spectrum, a digital oscilloscope (OSC) with a sample rate of 40 GS s^{-1} is used to record the time-domain waveforms, and an electrical spectrum analyzer (ESA) is applied to observe the RF spectrum.

As shown in figure 2(a), a TDC consists of several Gires–Tourno (G–T) etalons, and each G–T etalon made by silicon is a kind of optical interferometer, which consists of a perfectly reflective mirror and a partially reflective mirror with reflection coefficient r. Due to the interferometer effect, different frequencies experience different group delays in the cavity. The frequency-dependent group delay curve for each G–T etalon depends on the cavity length and reflectivity. The cavity length can be accurately controlled by precise temperature control. By cascading several G–T etalons, arbitrary dispersion curves can be generated. In this experiment, we use the TDC consisting of 16 G–T etalons to generate different dispersion curves and figure 2(b) shows two different dispersion curves as an example by setting the dispersion value at 0 and 2000 ps nm^{-1}, respectively.

The frequency response of the ith G-T etalon can be expressed in exponential form as:

$$H_i(\omega) = \exp\{i\varphi_i(\omega)\}, \tag{1}$$

where φ_i is the phase spectrum of the ith etalon, and can be described by [12]:

$$\varphi_i(\omega) = -arctg\frac{(1 - R_i)\sin\delta_i}{2\sqrt{R_i} - (1 + R_i)\cos\delta_i}, \tag{2}$$

where R_i is the reflectivity of the partially reflecting mirror in the ith etalon and δ_i is the phase shift of the optical beam in one round-trip of the ith cavity, which is decided by the cavity length. The function $arctg(\cdot)$ is the inverse tangent.

The TDC in the experiment consists of 16 G–T etalons, and the frequency response $H(\omega)$ is the multiplication of each

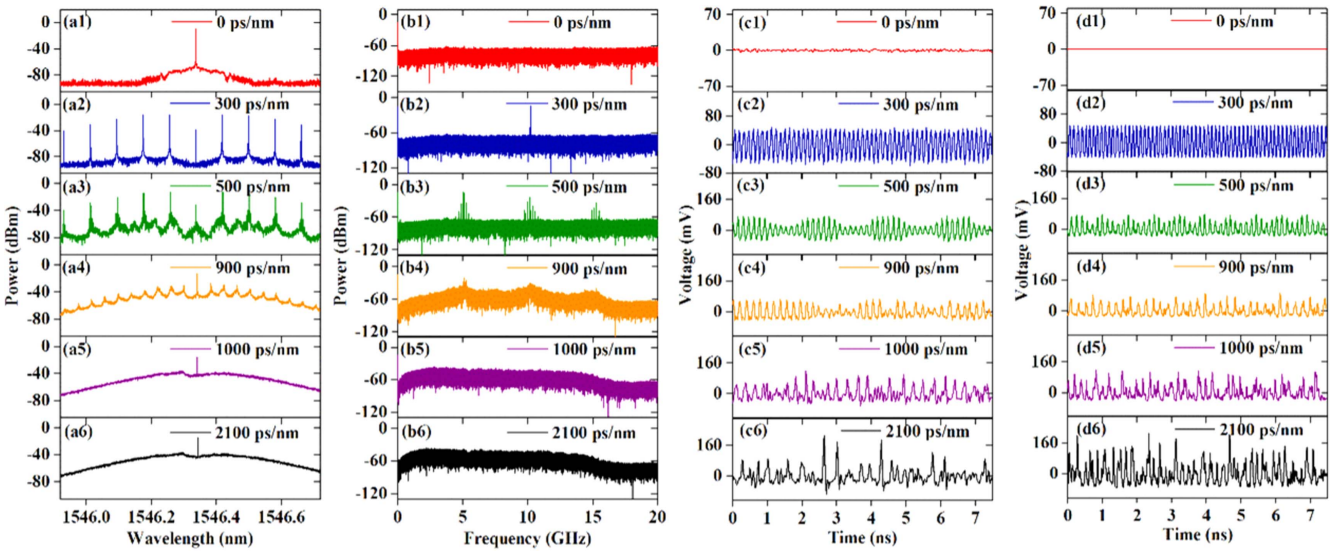

Figure 3. (a1)–(a6) Optical spectrum for different dispersion values in experiment, (b1)–(b6) RF spectrum for different dispersion values in experiment, (c1)–(c6) time-domain waveform for different dispersion values in the experiment, and (d1)–(d6) time-domain waveform for different dispersion values in the simulation.

etalon's frequency response, which can be expressed as:

$$H(\omega) = \prod_{i=1}^{16} H_i(\omega) = \exp\left\{i\sum_{i=1}^{16}\varphi_i(\omega)\right\} = \exp\{i\varphi(\omega)\}, \quad (3)$$

where $\varphi(\omega)$ is the phase spectrum of the TDC. The impulse response $h(t)$ of TDC is the reverse Fourier transform of the frequency response, which can be expressed as:

$$h(t) = F^{-1}\{\exp[i\varphi(\omega)]\}. \quad (4)$$

The optical phase changes proportionally to the voltage applied to the PM. Therefore, the complex electric field envelope at the PM output can be expressed as:

$$E(t) = E_0 \exp\left(i\frac{\pi V(t)}{V_\pi}\right), \quad (5)$$

where E_0 is the amplitude of the laser diode output, $V(t)$ is the output of the RF driver and V_π is the half-wave voltage of the PM.

The complex electric field envelop $E'(t)$ at the output of the TDC is the convolution between the complex field envelope at the PM output and the impulse response of the TDC, which can be expressed as:

$$E'(t) = E(t)^* h(t). \quad (6)$$

In the simulation, a finite impulse response (FIR) filter is used to simulate the impulse response of the TDC.

Therefore, a generalized dynamical model of the proposed phase chaos configuration can be described as:

$$V(t) + \tau\frac{dV(t)}{dt} + \frac{1}{\theta}\int_{t_0}^{t} V(t')dt' = \eta_0 GS\,|E'(t-T)|^2, \quad (7)$$

where G and S represent the gain of the RF driver and the sensitivity of the photodetector, respectively, and η_0 accounts for the overall cavity losses. The electrical response of the feedback loop is equivalent to a first-order band-pass filter, where $\upsilon_{hf} = (2\pi\tau)^{-1}$ and $\upsilon_{lf} = (2\pi\theta)^{-1}$ are the high cut-off frequency and low cut-off frequency of the equivalent band-pass filter, respectively.

The dynamical behavior can be performed via time series, RF spectra, and their corresponding optical spectra. The bifurcation of the behavior can be obtained by increasing the dispersion and the feedback gain. Figures 3(a1)–(a6) and (b1)–(b6) respectively show the optical and RF spectra in the experiment when the dispersion value is increased from 0 to 2100 ps nm^{-1}, and the injected optical power of PD is sustained at 0.3162 mW to ensure the feedback gain is unchanged. Figures 3(c1)–(c6) are the corresponding time-domain waveforms recorded by the OSC, and the corresponding time-domain waveforms in the simulation are shown in figures 3(d1)–(d6), which show good agreement with the experimental data. When the dispersion value is 0 ps/nm, as shown in figures 3(b1) and (c1), there is no oscillatory phenomenon in the frequency-domain and time-domain, and a single optical carrier can be observed in figure 3(a1). As the dispersion value is increased, a periodic oscillation can be observed in figure 3(c2), and the corresponding single frequency RF spectrum is shown in figure 3(b2). Meanwhile, the optical frequency comb is observed in figure 3(a2). When the dispersion keeps increasing, the quasi-period oscillation can be observed, the optical spectrum, RF spectrum and waveform are shown in figures 3(a3), (b3) and (c3), respectively. More frequency oscillations can be observed. As the dispersion increases to 900 ps nm^{-1}, a weak chaotic oscillation appears. As shown in figure 3(c4), the regular oscillation becomes unstable, and the peaks of the optical spectrum in figures 3(a4) become small because of the increasing floor level. When the dispersion value increases to 1000 ps nm^{-1}, chaotic oscillation become strong. As shown in figure 3(c5), the time-domain waveform becomes more irregular, the RF spectrum in figure 3(b5) becomes flatter, and the optical spectrum in figure 3(a5) becomes smooth. In addition, the

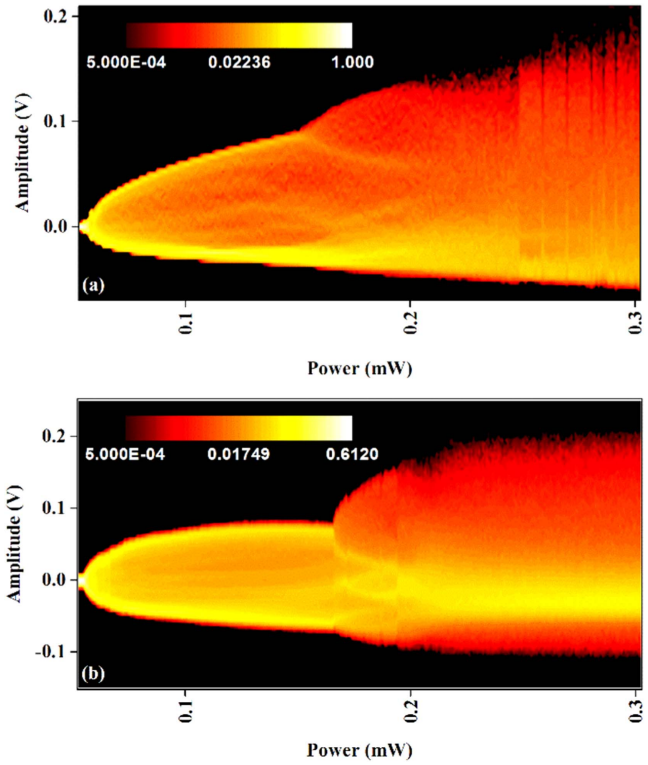

Figure 4. Bifurcation diagrams of the amplitude probability density function (logarithmic color scale) of the dynamics with respect to the injected optical power of PD. (a) From simulation data; (b) from experiment data.

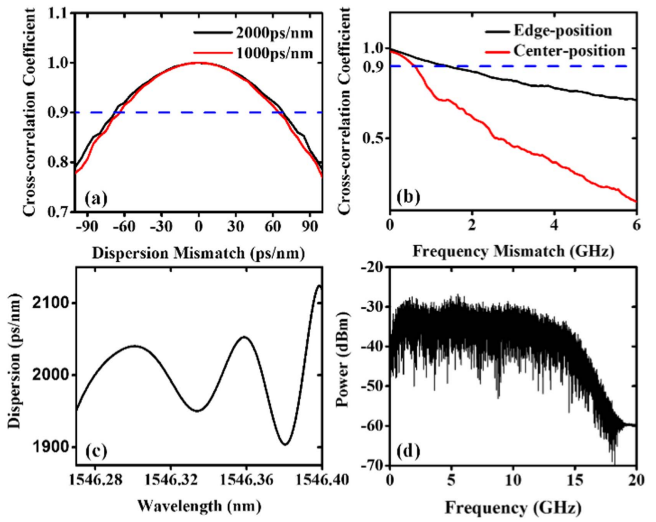

Figure 5. (a) Cross-correlation coefficient variation with dispersion value mismatch in the emitter and receiver, where the black and red lines respectively represent the 2000 ps nm^{-1} and 1000 ps nm^{-1} dispersion values in the emitter loop. (b) The cross-correlation coefficient variation with central frequency mismatch of each etalon in the TDC module for the irregular dispersion curve case, where black and red lines respectively represent the edge-positioned and center-positioned etalon case, (c) the irregular dispersion curve, and (d) the corresponding chaotic RF spectra.

chaotic states can be sustained when the dispersion value is increased to 2100 ps nm^{-1}, which is shown in figures 3(a6), (b6) and (c6). Note that 2100 ps nm^{-1} is the maximal setting dispersion value of the used TDC. Therefore, the change in the optical spectrum, RF spectrum and time-domain waveform as the increasing of dispersion value is an indication of the quasi-periodic route to chaos.

Furthermore, the amplitude probability density function (PDF) is used to represent the temporal dynamics. When the injected optical power of PD is finely tuned from 0 mW to 0.3162 mW to emulate the increase of the feedback gain, and the dispersion is sustained at 2100 ps nm^{-1}, a bifurcation diagram can be plotted to represent the evolution of the dynamics though its PDF with respect to the injected optical power of PD. The simulation and experimental results are shown in figures 4(a) and (b), respectively, where the PDF is encoded by the logarithmic color scaling, white means the highly probable amplitudes, red is the intermediate PDF amplitude, and dark represents the low probability amplitude. The time-domain series duration for the bifurcation diagram is about 0.5 μs at 40 GS s^{-1}, therefore, 20 000 points are used for the bifurcation diagram. This bifurcation diagram describes the optical phase dynamics from the stable steady state to the chaotic regime, while increasing the injected optical power of PD. Also, it can be noticed that the simulation and experimental results are in good agreement. The bifurcation scenario can be described as follows, when the injected optical power of PD is less than 0.0525 mW, the feedback gain is too small, therefore, the oscillator is nearly an open loop, and no oscillation can be observed. The zero amplitude is stable, which is not shown in figure 4. When the injected optical power of PD is increased from 0.0525 mW to 0.1663 mW, a two-level oscillation separated by a low probability amplitude band can be identified, which corresponds to periodic oscillation, and the two-level oscillation amplitude grows as the injected optical power is increased. Also, the multi-level quasi-periodic oscillation can be observed when the injected optical power is between 0.1663 mW and 0.1945 mW. For a higher injected optical power of PD, a washing out of the amplitude characteristic is observed, which corresponds to the chaotic oscillation, a typical waveform is shown in figure 3(c6).

After investigating the phase chaos generation based on the TDC in the feedback delayed-loop, we then evaluated the phase chaos synchronization by analyzing the synchronization error variation with a dispersion curve mismatch between the emitter and receiver. The synchronization error can be expressed as the cross-correlation coefficient between the waveforms in the emitter and receiver. The synchronization error is 0 when the cross-correlation coefficient is 1. Figure 5(a) shows the cross-correlation coefficient variation with the dispersion mismatch between the emitter and receiver for different dispersion values in the emitter. For both the 1000 ps nm^{-1} and 2000 ps nm^{-1} dispersion cases, the cross-correlation coefficient decreases as the dispersion mismatch value increases. When the dispersion mismatch value increases to 60 ps nm^{-1}, the cross-correlation coefficient decreases to 90%, which can define the fact that the phase chaos system cannot be synchronized. Therefore, the dispersion value can be considered as an additional key to enhance

the security level of the phase chaos system. Except for the fixed dispersion value, the used TDC module can also generate arbitrary dispersion curve by precisely controlling the temperature of each G-T etalon in the TDC [12]. The dispersion curve of TDC is the superposed dispersion curve of the cascading etalons, and the dispersion curve of each etalon can be controlled by shifting the central frequency through temperature tuning. Since it is difficult to quantitively evaluate the dispersion mismatch of an arbitrary dispersion curve, we use the central frequency mismatch of each etalon to replace the dispersion curve mismatch. The relationship between the cross-correlation coefficient and the central frequency mismatch of different etalons in TDC has also been investigated to evaluate the security level enhancement. Figure 5(b) shows the influence of central frequency mismatch for differently positioned etalons in the cross-correlation coefficient, where the black line represents the edge-positioned etalon, whose dispersion curve peak at the edge of the chaotic carrier spectrum, and the red line represents the center-positioned etalon, whose dispersion curve peak at the center of the chaotic carrier spectrum. According to figure 5(b), the cross-correlation coefficient decreases as the frequency mismatch increases in differently positioned etalons, and the cross-correlation coefficient decreases to 90% when the frequency mismatch increases to 1.4 GHz for an edge-positioned etalon, while it is only 0.6 GHz for a center-positioned etalon. Therefore, the frequency mismatch of the center-positioned etalon has a stronger influence in the cross-correlation coefficient than the edge-positioned etalon. To simply evaluate the key space, suppose the maximal frequency tuning range of each etalon in TDC is 20 GHz to cover the main part of the carrier spectrum, so one etalon can contribute at least 14 (20 GHz/1.4 GHz) key spaces to the security system for the edge-positioned etalon, and 16 cascaded etalons together can enlarge the key space by 14^{16} at least. When the frequency mismatch is zero in figure 5(b), the corresponding dispersion curve and chaotic RF spectrum are shown in figures 5(c) and (d), respectively. According to the chaotic RF spectrum in figure 5(d), the chaos state can still be sustained even when the dispersion curve is irregular.

In conclusion, by introducing a fine-controllable dispersion module into the delayed-feedback loop for nonlinear phase-to-intensity conversion, the phase chaos can be generated with high stability, and the chaos generation process is proved by both experimental demonstration and numerical simulation. Furthermore, the chaotic states can be sustained in a wide dispersion value range, so different dispersion curves can be used as a secure key, which significantly enhances the key space in the chaotic system. The dispersion curve in the emitter and receiver can be precisely tuned to any shape with a perfect match, therefore, the synchronization performance can be guaranteed. This research is expected to pave the way for the implementation of high-speed chaotic optical communication systems with enhanced security.

Funding

National Natural Science Foundation of China (NSFC) (61575122).

ORCID iDs

Lilin Yi https://orcid.org/0000-0002-6039-9063

References

[1] Pecora L M and Carroll T L 1990 Synchronization in chaotic systems *Phys. Rev. Lett.* **64** 821–4
[2] VanWiggeren G D and Roy R 1998 Communicating with chaotic lasers *Science* **279** 1198–200
[3] Fischer I, Liu Y and Davis P 2000 Synchronization of chaotic semiconductor laser dynamics on subnanosecond time scales and its potential for chaos communication *Phys. Rev.* A **62** 011801
[4] Sivaprakasam S and Shore K A 2000 Message encoding and decoding using chaotic external-cavity diode lasers *IEEE J. Quantum Electron.* **36** 35–9
[5] Annovazzi-Lodi V, Donati S and Scire A 1997 Synchronization of chaotic lasers by optical feedback for cryptographic applications *IEEE J. Quantum Electron.* **33** 1444
[6] Goedgebuer J P, Larger L and Porte H 1998 Optical cryptosystem based on synchronization of hyperchaos generated by a delayed feedback tunable laser diode *Phys. Rev. Lett.* **80** 2249
[7] Goedgebuer J P, Levy P, Larger L, Chen C C and Rhodes W T 2002 Optical communication with synchronized hyperchaos generated electrooptically *IEEE J. Quantum Electron.* **38** 1178–83
[8] Gastaud N, Poinsot S, Larger L, Merolla J M, Hanna M, Goedgebuer J P and Malassenet F 2004 Electro-optical chaos for multi-10 Gbit/s optical transmissions *Electron. Lett.* **40** 898–9
[9] Argyris A, Syvridis D, Larger L, Annovazzi-Lodi V, Colet P, Fischer I, Garcia-Ojalvo J, Mirasso C R, Pesquera L and Shore K A 2005 Chaos-based communications at high bit rates using commercial fibre-optic links *Nature* **438** 343–6
[10] Lavrov R, Peil M, Jacquot M, Larger L, Udaltsov V and Dudley J 2009 Electro-optic delay oscillator with nonlocal nonlinearity: optical phase dynamics, chaos, and synchronization *Phys. Rev.* E **80** 026207
[11] Lavrov R, Jacquot M and Larger L 2010 Nonlocal nonlinear electro-optic phase dynamics demonstrating 10 Gb/s chaos communications *IEEE J. Quantum Electron.* **46** 1430–5
[12] Hou T T, Yi L L, Yang X L, Ke J X, Hu Y, Yang Q, Zhou P and Hu W S 2016 Maximizing the security of chaotic optical communications *Opt. Express* **24** 23439–49